Int. J. Electrochem. Sci., 12 **(2017)** 2692 – 2703, doi: 10.20964/2017.04.23

International Journal of
ELECTROCHEMICAL
SCIENCE
www.electrochemsci.org

Synthesis of Porous Bowl-like $LiFePO_4$/C Composite with Ultrahigh Rate Capability

Boya Wang[1], *Lei Yao*[1], *Yan Wang*[2], *Jinhua Wu*[3], *Qiong Wang*[1], *Mingwu Xiang*[1], *Yun Zhang*[1], *Hao Wu*[1], *Heng Liu*[1,*]

[1] College of Materials Science and Engineering, Sichuan University, Chengdu, 610064, PR China;
[2] College of Computer Science and Technology, Southwest University for Nationalities, Chengdu, 610041, PR China;
[3] Department of Materials Engineering Sichuan College of Architectural Technology Deyang, 618000, P.R. China;
[*]E-mail: h_liu@scu.edu.cn

Received: 8 January 2017 / *Accepted:* 11 February 2017 / *Published:* 12 March 2017

Well-crystallized olivine-structure $LiFePO_4$/C composite was synthesized by a wet milling-assisted spray drying using cheap Fe_3O_4 as iron source. The composite exhibited bowl-like secondary particles that are mainly constructed of numerous carbon coated nanoparticles. Such a composite possesses a porous structure with an average pore size of 8.14 nm and a high BET surface area of 50.57 m^2 g^{-1}. Electrochemical tests revealed that the cathode material exhibited a high rate capability (84 mA h g^{-1} at 90 C) and good cycle stability (93% capacity retention over 500 cycles at 10 C). That is because the uniform carbon coating increased the electronic conductivity, while, large specific surface area, porous structure, and nano-sized particles greatly favored the electrolyte accessibility and rapid Li^+ transport.

Keywords: lithium ion battery; cathode material; $LiFePO_4$/C composite; rate performance

1. INTRODUCTION

Since olivine-structured lithium iron phosphate ($LiFePO_4$) was proposed as a new-type cathode material for lithium ion batteries, it has attracted tremendous research due to its high theoretical capacity (170 mAh g^{-1}), good cycling stability, low cost and environmental friendliness [1, 2]. However, with the deepening of the research, two main defects have aroused much concern. $LiFePO_4$ without modification exhibits a low electric conductivity and slow lithium ion diffusion rate, directly leading to a terrible rate performance, hindering its large scale applications on electric vehicle (EVs) and hybrid electric vehicles (HEVs).

Hence, considerable researches have made great efforts in enhancing the rate performance of $LiFePO_4$, such as optimizing particle size [3, 4], coating conductive carbon [5, 6], doping supervalent cations [7, 8] and modifying morphology [9, 10]. The fact proved that conductive carbon layer coating is the most feasible method to boost the electronic conductivity of $LiFePO_4$ because of its abundant material supply and facile fabrication procedure. However, only with carbon coating or additive is impossible to obtain superior high rate performance [11]. So, a $LiFePO_4$/C composite consisting of carbon coating, nano-sized $LiFePO_4$ particles with porous structure, which can provide fast electronic conduction and lithium ion transport, receives much concern. A. Kotov et al. [12] synthesized a high surface area 3D hierarchical $LiFePO_4$/C composite coated by reduced graphene oxide networks via layer-by-layer assembly, which exhibited a stable discharge capacity of 56 mAh g^{-1} at 160 C. Chen et al. [13] prepared a high surface area and abundant pore structure $LiFePO_4$/C composite by an in situ polymerization restriction method, which displayed a discharge capacity of 62.8 mAh g^{-1} at 50 C. However, the preparation methods mentioned above still suffer from some obstacles in general application. One is the expensive reaction reagent; the other is the complex synthetic procedure with low yield. Thus, a novel synthesis approach with low cost and facile synthetic process, which can produce $LiFePO_4$/C with superior high rate performance, is exploited urgently.

In this study, well-crystallized olivine-structure $LiFePO_4$/C composite was synthesized via a facile wet milling-assisted spray drying method using low cost Fe_3O_4 as the iron source and cheap glucose as the carbon source and reductive agent. The composite displays porous bowl-like $LiFePO_4$/C secondary particles with a size ranging from 2 to 6 μm in diameter that are constructed of numerous carbon coated nanoparticles. The carbon coating increased the electronic conductivity, meanwhile, porous structure and nano-sized primary particles facilitated Li^+ diffusion. Hence, the as-prepared $LiFePO_4$/C composite material displays good electrochemical properties, especially the rate performance.

2. EXPERIMENTAL DETAILS

2.1 Materials Preparation

As described in Fig. 1, $LiFePO_4$/C composite was prepared by a wet milling-assisted spray drying method. In a typical process, 15.00 g Fe_3O_4 was homogeneously dispersed in 150 ml water solution followed by the addition of 7.372 g H_3PO_4 (85 wt%) solution, and then reacted in 95 °C for 5 h. After reacting, the slurry was transferred into a milling jar followed by the addition of 2.718 g $LiOH{\cdot}H_2O$ and appropriate glucose (the mass ratio of $LiFePO_4$ to glucose was 100:15) to mill. The obtained suspension was spray-dried in a spray-drying unit, followed by annealing at 600 °C for 10 h in a nitrogen atmosphere to generate porous bowl-like $LiFePO_4$/C composite (LFP/C). Notably, washing was not needed during the whole synthesis processes; therefore, there was no liquid waste to produce. Thus, the preparation method mentioned above is eco-friendly and water saving, which are very important for industrial production. Commercial $LiFePO_4$/C sample (Commercial LFP/C) was purchased from Tianjin Sterlan-Energy Ltd., China.

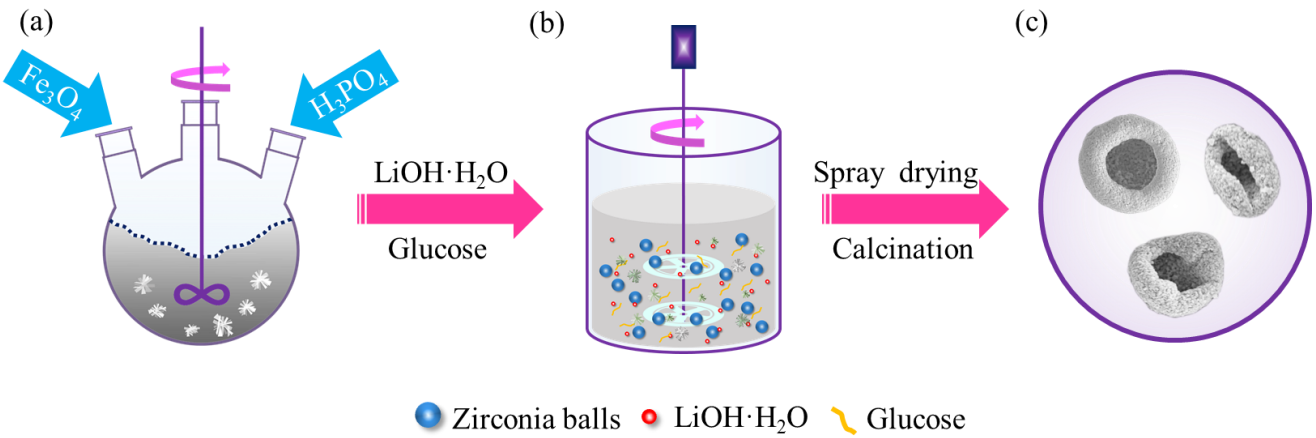

Figure 1. Schematic representation of the synthesis procedure of bowl-like $LiFePO_4$/C composite.

2.2 Materials Characterization

The crystalline phases of synthesized $LiFePO_4$/C composite were identified by X-ray diffraction (XRD, Philips X'pert TROMPD, Cu Kα1 radiation, λ=1.54178 Å). The Raman spectra were recorded on a Raman spectrophotometer (Horiba Jobin Yvon, HR800, France) with 532.17 nm laser radiation in the range of 100-2000 cm^{-1}. The morphology and microstructure of the sample were examined by a field emission scanning electron microscopy (FE-SEM, Hitachi, S-4800, Japan) and a field emission transmission electron microscopy (TEM, FEI, Titan themis 200, USA). Nitrogen adsorption/desorption isotherms and pore size distribution were characterized by Kubo-X1000 analyzer (Beijing Builder Electronic Technology Co., Ltd). The surface area was calculated by the Brunauer-Emmett-Teller (BET) method. And the pore size distributions were derived from the desorption branches of isotherms using the Barrett-Joyner-Halenda (BJH) model. The total pore volume was calculated at a relative pressure of 0.99 (P/P_o). The carbon contents in the $LiFePO_4$/C sample were tested by chemical analysis.

2.3 Electrochemical measurements

To evaluate the electrochemical performance of the $LiFePO_4$/C composite as cathode for lithium ion batteries, CR2032 coin-type cells were assembled in an argon-filled glove box using lithium foil as counter electrode and Celgard 2400 as separator, respectively. The cathode slurry was prepared by mixing 80 wt% $LiFePO_4$/C composite, 10 wt% acetylene black and 10 wt% polyvinylidene fluoride (PVDF) in 1-methyl-2-pyrrolidinone (NMP), and then coated on Al foil dried at 120 °C in a vacuum for 12 h. The final sheet was punched into disc (Φ=14 mm) as the working electrode. The electrolyte is consisted of a solution of 1 M $LiPF_6$ in ethylene carbonate (EC)/dimethyl carbonate (DMC) (1:1 by volume). The charge and discharge performance was determined by an automatic NEWARE battery cycler (Neware, China) in a voltage range of 2.5-4.3 V at room temperature. Cyclic voltammetry (CV) were conducted by a PARSTAT multichannel electrochemical workstation (Princeton Applied Research, PMC1000DC, USA) at a scanning rate of 0.1 mV s^{-1}

between 2.5 and 4.3 V (vs Li/Li^+). Electrochemical impedance spectra (EIS) were performed by a PARSTAT electrochemical workstation (Princeton Applied Research, PMC1000, USA), using an AC voltage of 5 mV amplitude in the frequency range from 100 KHz to 0.1 Hz.

3. RESULTS AND DISCUSSION

3.1 Structural characterizations and Morphologies

Fig. 2a shows the XRD patterns of LFP/C. It can be identified to be an orthorhombic olivine structure (JCPDS card no. 83-2092) with a space group of *Pnma*. The diffraction peaks of LFP/C were strong and narrow, suggesting a high crystallinity of $LiFePO_4$. No diffraction peaks corresponding to detectable impurity phases (such as Li_3PO_4 [14] and Fe_2P [15]) were detected. In addition, the diffraction peaks of carbon were not detected, showing the carbon was amorphous. Elemental analysis revealed that the average carbon content was 4.53 wt% for LFP/C. Raman experiment was also conducted to characterize the structure of LFP/C. The peaks between 200 and 1100 cm^{-1} can be assigned to the $LiFePO_4$ lattice. These vibrational bands were in accordance with the assignments reported in the literature, indicating the high purity of $LiFePO_4$ [16]. The Raman spectra show two intense and broad bands located at ~1331 and ~1600 cm^{-1}, respectively, which are ascribable to the D (disordered) and G (graphene) bands of carbon. The I_D/I_G ratio of LFP/C is 0.87. The low intensity ratio of I_D/I_G indicates more graphene clusters in the structure of carbon, which would increase the electronic conductivity of the carbon and improve the utilization of $LiFePO_4$ in the cathode [17].

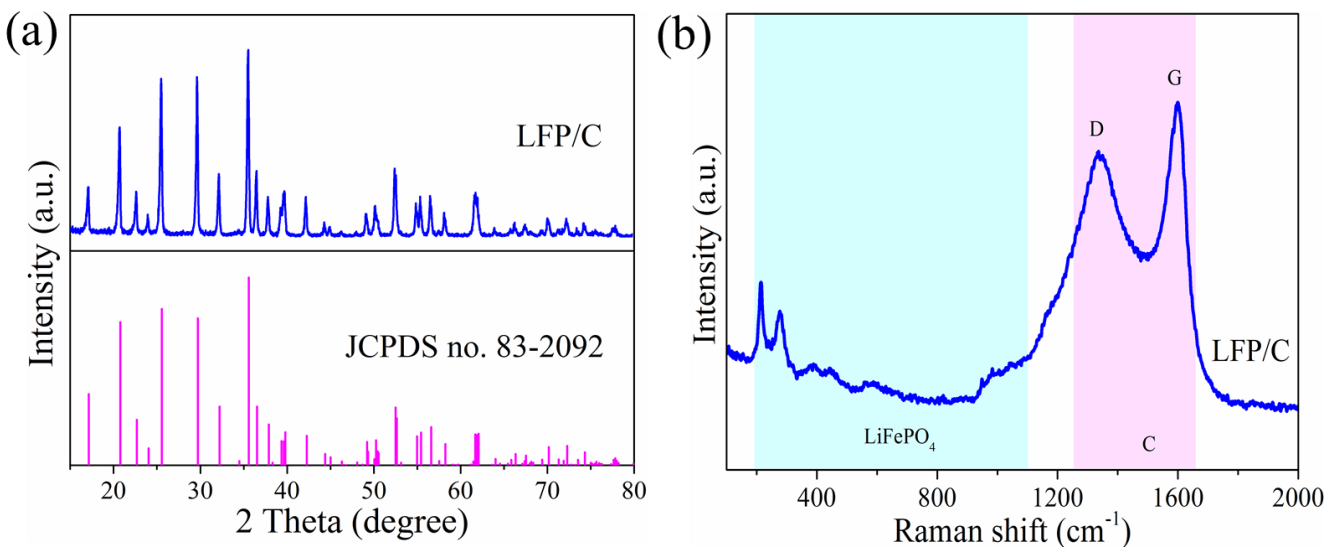

Figure 2. (a) XRD patterns of LFP/C and the standard $LiFePO_4$ (JCPDS card no. 83-2092); (b) Raman spectra of LFP/C.

Fig. 3 presents the morphology and microstructure of LFP/C. The SEM images display bowl-like LFP/C secondary particles with a size ranging from 2 to 6 μm in diameter. The bowl-like

$LiFePO_4$/C composite results from the deformation of the initial spherical shape of the droplets formed by the nebulizer [18, 19]. It is worth noting that the obtained bowl-like LFP/C were constructed of numerous nanoparticles (≤ 100 nm). The LFP/C presented abundant pore structures on the surface, which were attributed to the release of H_2O and CO_x during the calcination process [13]. The nitrogen isothermal adsorption/desorption measurements were conducted for further investigating the porous structure of LFP/C (Fig. S1). The isotherm curves of LFP/C show a type IV curve based on IUPAC classification with a steep increase of nitrogen absorption at a high relative pressure (P/P_0=0.8-0.99), suggesting that the most pore volume is caused by mesoporous [19-21]. In addition, analyzing the pore size distribution can further verify the pore structure of the sample. As seen in Fig. S1, LFP/C showed a main pore size distribution in the range of 2-20 nm, confirming that the sample was of typical mesoporous structures. And, it shows a high Brunauer-Emmett-Teller (BET) specific surface area of 50.57 $m^2 g^{-1}$ and a large pore volume of 0.206 $cm^3 g^{-1}$ (P/P_o=0.99). The higher specific surface area and pore volume of LFP/C would provide plenty of sites for interfacial contact with the electrolyte and facilitate the transport of electrons and lithium ions in the electrode, thus reducing the electrode concentration polarization and improving the rate performance [22-24].

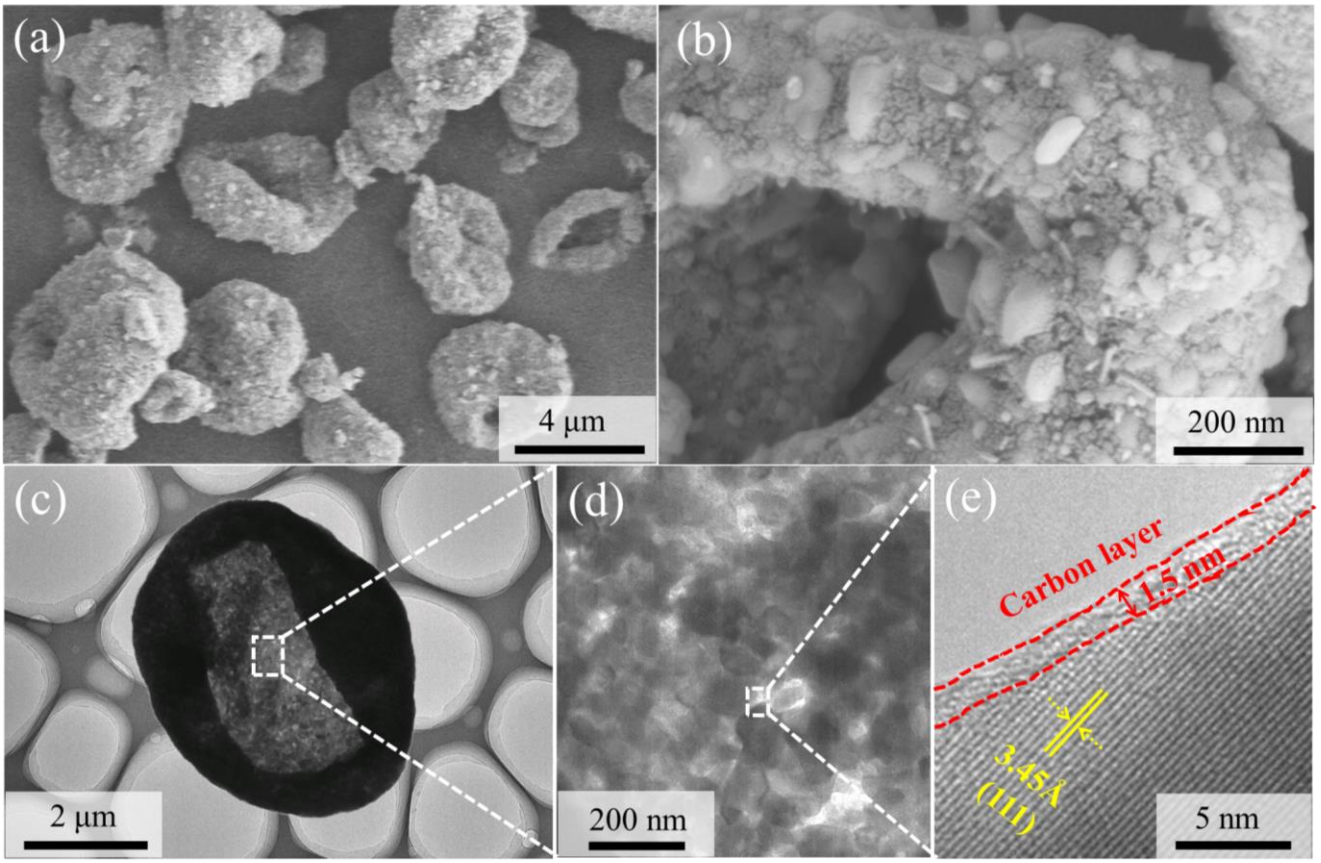

Figure 3. (a, b) SEM images of LFP/C at different magnifications; (c, d) TEM image of LFP/C; (f) HRTEM image of LFP/C.

TEM and high resolution TEM (HRTEM) observations were carried out for further insight into the microstructure of LFP/C. It can be seen that the bowl-like LFP/C showed porous structure (Fig. 3c, d), which was corresponded to the result of nitrogen isothermal adsorption/desorption measurements. The HRTEM image shows that a uniform and thin carbon layer (~1.5 nm) coated on the surface of the $LiFePO_4$ particles. The lattice fringes with the spacing of 3.45 Å correspond to the (111) plane of $LiFePO_4$ for the sample, which also indicated a good crystallization of the material. This porous bowl-like LFP/C constructed by carbon coated nano-sized $LiFePO_4$ particles can greatly facilitate the transport of electron and Li^+, which can dramatically enhance the rate performance.

3.3 Electrochemical characterization

The commercial LFP/C product (Fig. S1, S2) was used to illustrate the good electrochemical performance of LFP/C. Fig. 4a exhibits their galvanostatic charge-discharge curves at a low current rate of 0.2 C. The charge-discharge plateaus of two samples were around 3.40 V, which were corresponding to the Fe^{2+}/Fe^{3+} transformation [9]. Commercial LFP/C and LFP/C exhibited reversible capacity of 156.4 and 163.2 mAh g^{-1}, respectively. As shown in the inset of Fig. 4a, the polarization values between the charge and discharge plateaus of LFP/C were smaller than that of commercial LFP/C, suggesting an enhanced reaction kinetics, which was attributed to the large specific surface area, porous structure, and carbon coated nanoparticles of LFP/C. With the increase of current rate, the LFP/C presented a higher discharge capacity of 135, 127, and 120 mAh g^{-1} at 5, 10, and 20 C, respectively, while commercial LFP/C only exhibited 120, 103, and 49 mAh g^{-1} at the corresponding current rates. It is worth noting that the LFP/C even could discharge capacity of 110 mAh g^{-1} at 45 C and 84 mAh g^{-1} at 90 C, but the commercial LFP/C was almost failed at these current rates. In addition, more stable potential plateau during high current rate for LFP/C (Fig. 4d) indicated both the higher energy density and power density [25]. The good rate capability of LFP/C could be attributed to the good crystallization as well as the enhanced electronic conductivity and Li^+ diffusion rate originated from the special microstructure and small particle size. Fig. 4e exhibits the cycle performance of the samples at 10 C. The LFP/C exhibited a good cycling stability throughout the continuous charge-discharge process with capacity retention of 93.0% after 500 cycles (with a reversible capacity of 118 mAh g^{-1}). The corresponding average Coulombic efficiency reached 99.6%, indicating the highly reversible Li^+ insertion/extraction kinetics [26]. However, the commercial LFP/C only retained 67.7% of initial capacity after 500 cycles (with a reversible capacity of 67.3 mAh g^{-1}). The good cycling performance of LFP/C may results from the stable structure and a coating of uniform and thin carbon layer.

The cyclic voltammograms (CV) of the samples at a scan rate of 0.1 mV s^{-1} are shown in Fig. 5a. Both of samples showed a couple of redox peaks around 3.4 V vs. Li^+/Li, corresponding to the Li^+ insertion/extraction in the $LiFePO_4$ crystal [27].

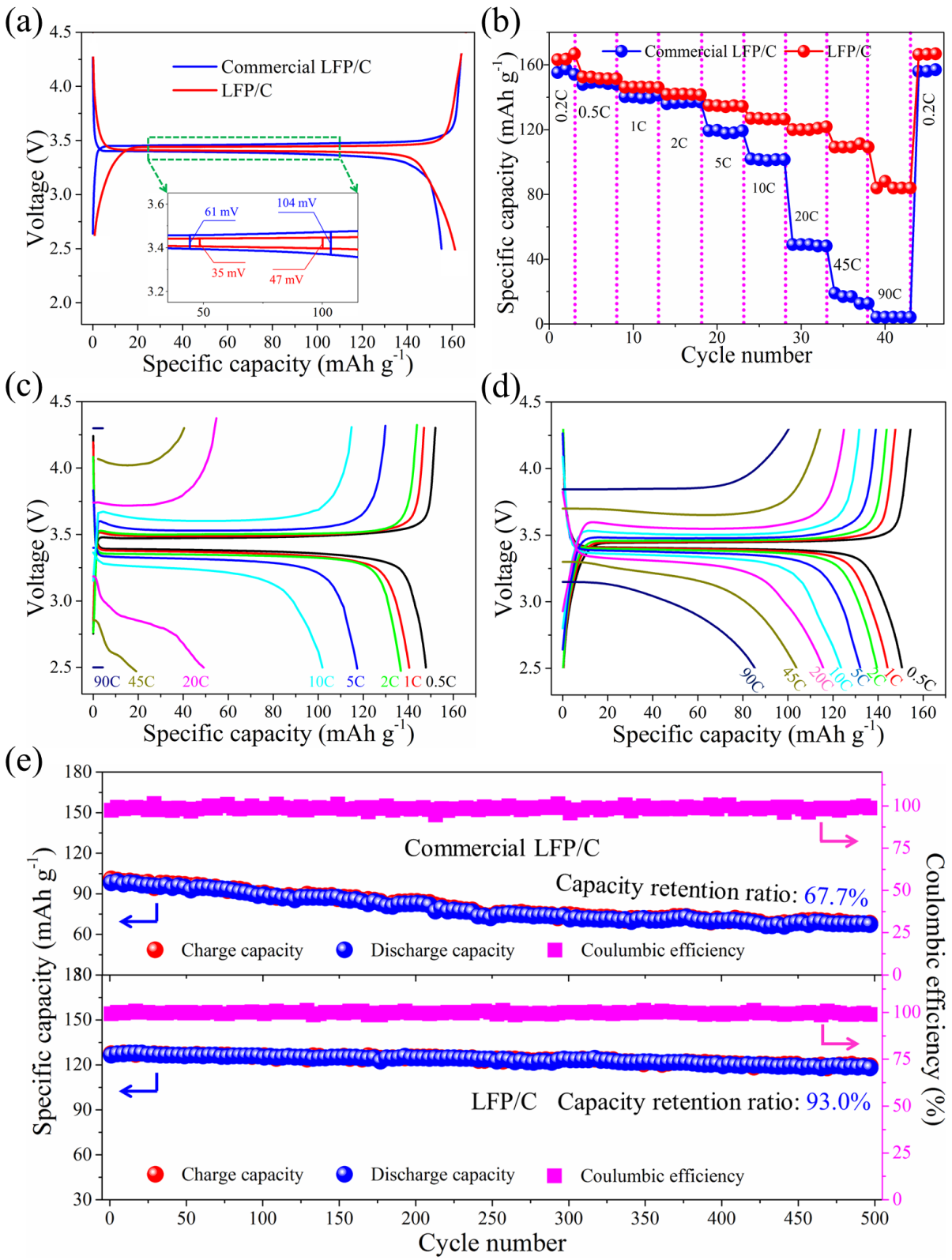

Figure 4. (a) charge/discharge profiles at 0.2 C, inset: the magnified selected-region comparing the potential plateaus; (b) discharge capacities at various rates of Commercial LFP/C and LFP/C; (c, d) charge/discharge profiles at current rates ranging from 0.5 C to 90 C; (e) cycling performance combined with Coulombic efficiency at 10 C of commercial LFP/C and LFP/C.

The redox peaks of LFP/C were more symmetric and spiculate than that of commercial LFP/C, indicating a good reversibility of lithium insertion/extraction reactions and higher electrode kinetics. The potential interval between the two redox peaks of commercial LFP/C and LFP/C were 231 mV and 157 mV, respectively. The smaller potential interval confirms the improved reversibility and reactivity of LFP/C, which account for its superior rate performance.

Fig. 5b shows the electrochemical impedance spectroscopy (EIS) in the frequency range from 0.1 Hz to 100 kHz. The EIS can be divided to two segments: a semicircle at high frequency and an inclined line within the low frequency range. The resistance of the semicircle is attributed to the charge transfer process. It is indicated that LFP/C composite showed a smaller charge transfer resistance (40.11 Ω) than that of commercial LFP/C (108.1 Ω), indicating improved charge transferring and reaction kinetics by mesoporous bowl-like structure and the uniform carbon coating. The Nyquist plots were fitted using the equivalent circuit (shown in the inset of Fig. 5b) and the fitting results were presented in Table 1. The inclined lines were attributed to the diffusion of the lithium ions into the bulk of the electrode material, the so-called Warburg diffusion (σ), which can be obtained by equation (1): [28]

$$Z_{re} = R_e + R_{ct} + \sigma\omega^{-1/2} \quad (1)$$

where R_e is the resistance of the electrolyte, R_{ct} is the charge transfer resistance and the ω is the angular frequency in the low frequency region. Both R_e and R_{ct} are kinetics parameters independent of frequency. So, σ is the slope for the plot of Z_{re} vs. the reciprocal root square of the angular frequencies ($\omega^{-1/2}$). The plot of Z_{re} vs. the reciprocal root square of the lower angular frequencies ($\omega^{-1/2}$) for the samples is shown in Fig. 5c. In addition, the Li^+ diffusion coefficient (D) are determined by the following equation (2): [29, 30]

$$D=R^2T^2/2A^2n^4F^4C^2\sigma^2 \quad (2)$$

where R is the gas constant (8.314 J mol^{-1} K^{-1}), T is the absolute temperature (298.15 K), n is the charge transfer number per molecule during intercalation, and F is the Faraday constant (96 486 C mol^{-1}), A is the surface area of the cathode, C is the concentration of lithium ion. The Li^+ diffusion coefficient of commercial LFP/C and LFP/C were 1.05×10^{-14} and 1.25×10^{-13} cm^2 s^{-1}, respectively, as shown in Table 1. The lowered charge transfer resistance and increased Li^+ diffusion coefficient of LFP/C greatly favored its superior rate capability.

Table 1. The resistance and lithium-ion coefficient of commercial LFP/C and LFP/C.

Samples	R_e (Ω)	R_{ct} (Ω)	D (cm^2 s^{-1})
Commercial LFP/C	7.289	108.1	1.05×10^{-14}
LFP/C	2.588	40.11	1.25×10^{-13}

Table 2 compares the bowl-like LFP/C with similar cathode materials that were described in literature. It can be seen that the synthesis method of this work is facile and the bowl-like LFP/C exhibit good rate performance. The better rate capability of the bowl-like LFP/C also clearly can be seen in Fig. 5d, which exhibits the rate performance of LFP/C and some previously reported $LiFePO_4$ composites [5, 13, 15, 24, 31-38]. This excellent rate performance may be ascribed to the high

electronic conductivity, which was originating from the uniform carbon coating, and increased Li^+ diffusion coefficient, which was owing to the special microstructure and nano-sized primary particles. This also can be supported by the result of EIS measurement. It is worth nothing that the LFP/C/RGO [37] exhibited better rate performance than our work in the low and middle rate. However, the usage of reduced graphene oxide also made it suffer from obstacles related to expensive materials for large-scale applications.

Table 2. Comparison of the bowl-like LFP/C composite with similar cathode materials.

Ref.	Synthesis	Structure	Active material (%)	Carbon content (%)	binder/carbon black (%/%)	rate (C)	Capacity (mAh g^{-1})
5	co-precipitation + spray drying	porous $LiFePO_4$/C microspheres	83	8.4	10/7	0.1 10 20	163 100 80
13	polymerization restriction method	porous $LiFePO_4$/C nanocomposite	80	10.2	10/10	0.5 10 50	156 109 63
15	supercritical alcohol route	hierarchically porous $LiFePO_4$ microspheres	70	6.1	20/10	0.1 10 40	160 115 50
19	wet milling-spray drying-carbothermal reduction	mesoporous bowl-like $LiFePO_4$/C composites	80	2.4	10/10	0.5 10 20	162 124 106
24	sol–gel proces	hierarchical porous C/$LiFePO_4$/C composite	80	8.9	10/10	0.5 10 40	144 93 69
31	microwave-assisted hydrothermal approach + carbothermal reduction	monodisperse porous $LiFePO_4$/C microspheres	80	9.17	10/10	0.1 10	146 90
33	solvothermal route + catalytic synthesis	high-graphitized carbon coated $LiFePO_4$ nanoplates	80	5.8	10/10	0.2 10 100	170 141 65
35	solvothermal method + hydrothermal treatment	three-dimensional porous $LiFePO_4$	80	15.4	10/10	0.2 10 100	155 124 78
37	hydrothermal treatment	LFP nanorods encapsulated conformal carbon and RGO	85	2	5/10	0.1 10	172 142
38	hydrothermal treatment	$LiFePO_4$ nanomesh	90	-	5/5	0.1 10 20	161 116 96
This work	wet milling + spray drying	porous bowl-like LFP/C	80	4.5	10/10	0.1 10 90	163 127 84

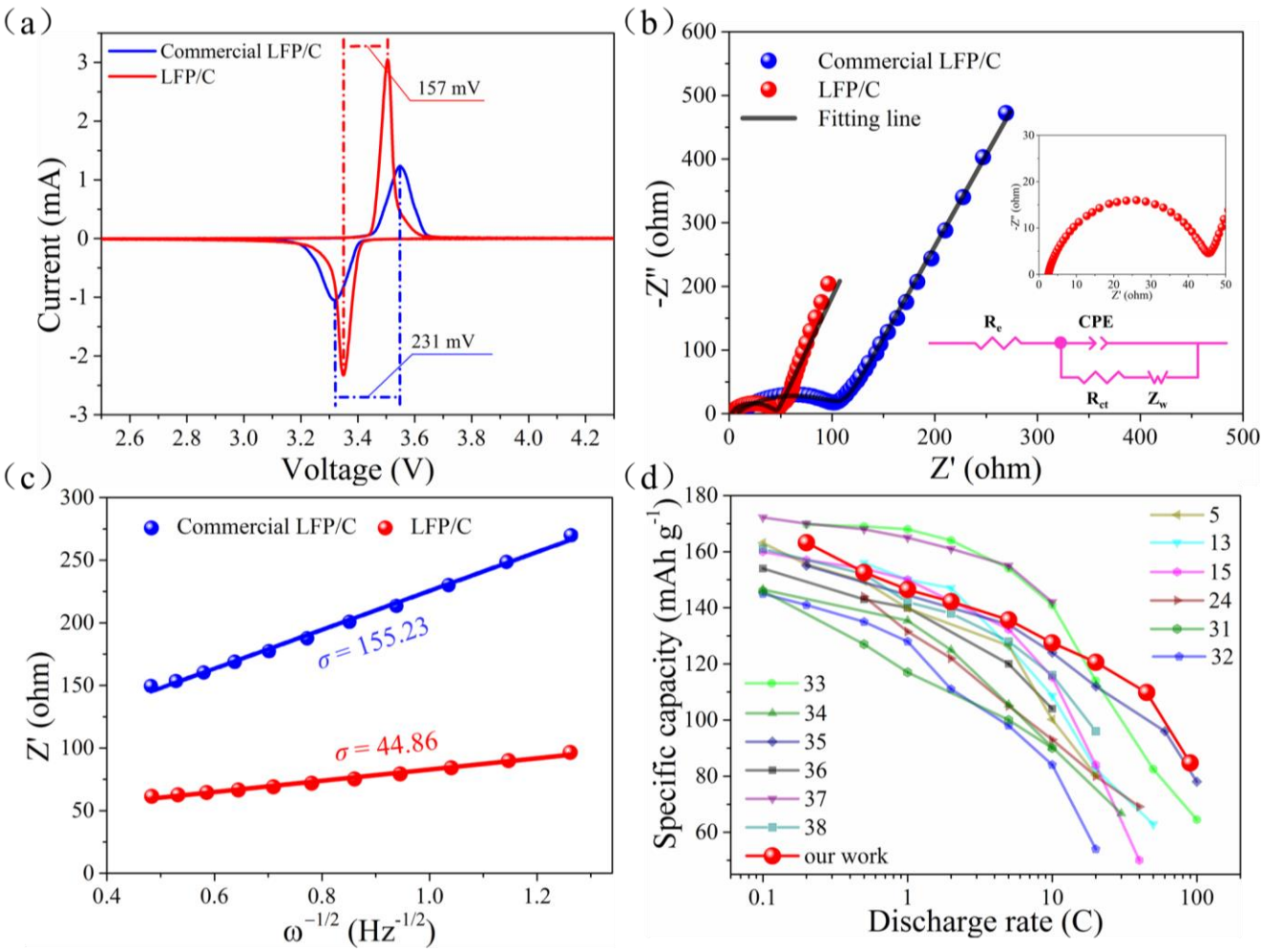

Figure 5. (a) The CV curves at a scan rate of 0.1 mV s^{-1}; (b) EIS plots and equivalent circuit of Commercial LFP/C and LFP/C; (c) The relationship between resistance (Z_{re}) and Frequency square root ($\omega^{-1/2}$); (d) Comparison of the rate capability of LFP/C with some previously reported $LiFePO_4$/C composites.

4. CONCLUSION

In this study, well-crystallized olivine-structure $LiFePO_4$/C composite was successfully synthesized by a wet milling-assisted spray drying using cheap Fe_3O_4 as iron source. The composite exhibited a particle size of 2-6 μm in diameter and shown porous bowl-like morphology with a high specific surface area of 50.57 m^2 g^{-1} and an average pore volume of 0.207 cm^3 g^{-1}. Electrochemical tests revealed that LFP/C even could discharge capacity of 110 mAh g^{-1} at 45 C and 84 mAh g^{-1} at 90 C. It also exhibited a good cycling stability (93% capacity retention over 500 cycles at 10 C). The enhanced rate capacity and cycle performance were mainly ascribed to the porous structure with high specific surface area, nano-sized particles and uniform carbon coating, which improved the ionic/electronic conductivity collectively. Hence, the method for preparing porous bowl-like LFP/C composite described in this paper is a cost-effective and efficient approach, which can be applied to the mass production of high performance $LiFePO_4$/C.

SUPPORTING INFORMATION:

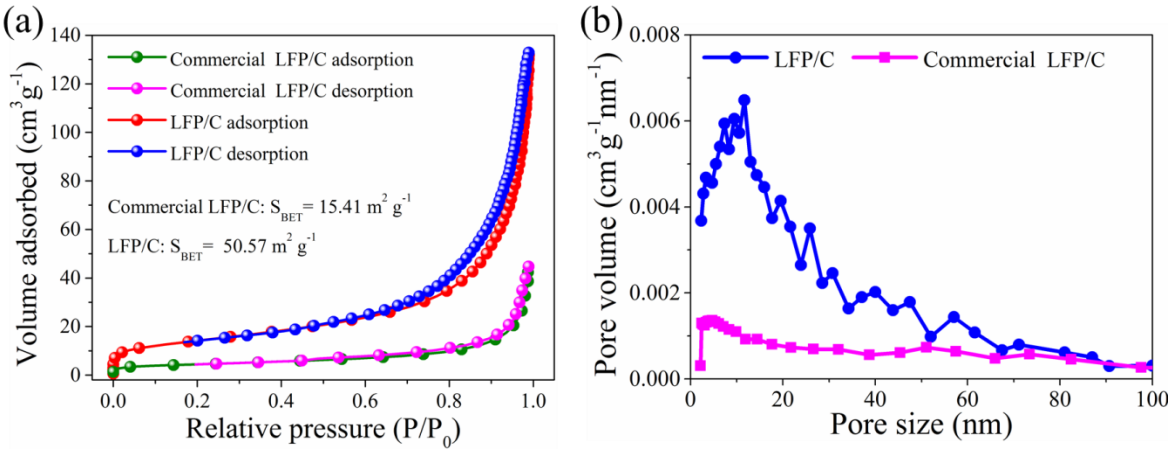

Figure S1. (a) Nitrogen adsorption/desorption isotherms and (b) the corresponding pore size distribution curves calculated by the BJH formula from desorption branch isotherm of commercial LFP/C and LFP/C, respectively.

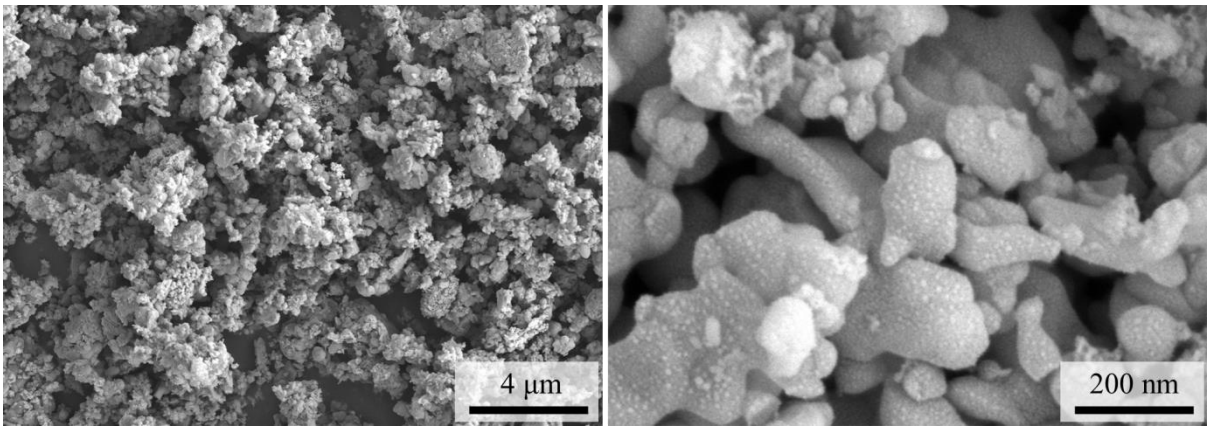

Figure S2 (a) SEM images of commercial LFP/C, revealing that the particles are in irregular in shape with particle size ranging from tens of nm to hundreds of nm. Severe particle agglomeration can also be seen.

ACKNOWLEDGEMENT
This work was supported by the Sichuan Province Science & Technology Foundation of China (2014GZ0094).

References

1. A. K. Padhi, K. S. Nanjundaswamy, J. B. Goodenough, *J. Electrochem. Soc.*, 144 (1997) 1188-1194.
2. S. Bolloju, R. Rohan, S.-T. Wu, H.-X. Yen, G. D. Dwivedi, Y. A. Lin, J.-T. Lee, *Electrochim. Acta*, 220 (2016) 164-168.
3. Y. Liu, M. Zhang, Y. Li, Y. Hu, M. Zhu, H. Jin, W. Li, *Electrochim. Acta*, 176 (2015) 689-693.
4. K. Vediappan, A. Guerfi, V. Gariépy, G. P. Demopoulos, P. Hovington, J. Trottier, A. Mauger, C. M. Julien, K. Zaghib, *J. Power Sources*, 266 (2014) 99-106.

5. D. Xu, X. Chu, Y.-B. He, Z. Ding, B. Li, W. Han, H. Du, F. Kang, *Electrochim. Acta*, 152 (2015) 398-407.
6. S. Uchida, M. Yamagata, M. Ishikawa, *J. Power Sources*, 243 (2013) 481-487.
7. I. D. Johnson, E. Blagovidova, P. A. Dingwall, D. J. L. Brett, P. R. Shearing, J. A. Darr, *J. Power Sources*, 326 (2016) 476-481.
8. I. D. Johnson, M. Lübke, O. Y. Wu, N. M. Makwana, G. J. Smales, H. U. Islam, R. Y. Dedigama, R. I. Gruar, C. J. Tighe, D. O. Scanlon, F. Corà, D. J. L. Brett, P. R. Shearing, J. A. Darr, *J. Power Sources*, 302 (2016) 410-418.
9. N. Bai, K. Xiang, W. Zhou, H. Lu, X. Zhao, H. Chen, *Electrochim. Acta*, 191 (2016) 23-28.
10. G. Wang, Z. Ma, G. Shao, L. Kong, W. Gao, *J. Power Sources*, 291 (2015) 209-214.
11. G. Qin, Q. Ma, C. Wang, *Electrochim. Acta*, 115 (2014) 407-415.
12. R. Mo, S. O. Tung, Z. Lei, G. Zhao, K. Sun, N. A. Kotov, *ACS Nano*, 9 (2015) 5009-5017.
13. J. Chen, N. Zhao, G.-D. Li, F.-F. Guo, X. Wang, T. Jia, J. Zhao, Y. Zhao, X. Wang, L. Wan, *Mater. Chem. Phys.*, 180 (2016) 244-249.
14. K. S. Dhindsa, A. Kumar, G. A. Nazri, V. M. Naik, V. K. Garg, A. C. Oliveira, P. P. Vaishnava, Z. X. Zhou, R. Naik, *Solid State Electr.*, 20 (2016) 2275-2282.
15. W. Li, J. Hwang, W. Chang, H. Setiadi, K. Y. Chung, J. Kim, *J. Supercrit. Fluids*, 116 (2016) 164-171.
16. L. Wang, X. He, W. Sun, J. Wang, Y. Li, S. Fan, *Nano Lett.*, 12 (2012) 5632-5636.
17. G. T.-K. Fey, K.-P. Huang, H.-M. Kao, W.-H. Li, *J. Power Sources*, 196 (2011) 2810-2818.
18. S. H. Luo, Z. L. Tang, J. B. Lu, Z. T. Zhang, *Chinese Chemical Letters*, 18 (2007) 237-240.
19. Y. Lv, Y. Long, J. Su, X. Lv, Y. Wen, *Electrochimica Acta*, 119 (2014) 155-163.
20. X. Huang, B. Sun, K. Li, S. Chen, G. Wang, *J. Mater. Chem. A*, 1 (2013) 13484-13489.
21. Q.-B. Liu, S.-J. Liao, H.-Y. Song, Z.-X. Liang, *J. Power Sources*, 211 (2012) 52-58.
22. V. Anh, Y. Qian, A. Stein, *Adv. Energy Mater.*, 2 (2012) 1056-1085.
23. Y. H. Chen, C. W. Wang, X. Zhang, A. M. Sastry, *J. Power Sources*, 195 (2010) 2851-2862.
24. J. Song, L. Wang, Z. Ma, Z. Du, G. Shao, L. Kong, W. Gao, *Rsc Adv.*, 5 (2015) 1983-1988.
25. X. Wu, Y. Guo, J. Su, J. Xiong, Y. Zhang, L. Wan, *Adv. Energy Mater.*, 3 (2013) 1155-1160.
26. J. Liu, T. E. Conry, X. Song, M. M. Doeff, T. J. Richardson, *Energ. Environ. Sci.*, 4 (2011) 885.
27. Q. Zhang, S.-Z. Huang, J. Jin, J. Liu, Y. Li, H.-E. Wang, L.-H. Chen, B.-J. Wang, B.-L. Su, *Scientific Reports*, 6 (2016) 25942.
28. Y. Cui, X. Zhao, R. Guo, *Electrochim. Acta*, 55 (2010) 922-926.
29. A. Y. Shenouda, H. K. Liu, *J. Power Sources*, 185 (2008) 1386-1391.
30. K. Tang, X. Yu, J. Sun, H. Li, X. Huang, *Electrochim. Acta*, 56 (2011) 4869-4875.
31. R. Chen, Y. Wu, X. Y. Kong, *J. Power Sources*, 258 (2014) 246-252.
32. H. Fei, Z. Peng, Y. Yang, L. Li, A. R. Raji, E. L. Samuel, J. M. Tour, *Chem. Commun.*, 50 (2014) 7117-7119.
33. Z. Ma, Y. Fan, G. Shao, G. Wang, J. Song, T. Liu, *ACS Appl. Mater. Interface*, 7 (2015) 2937-2943.
34. J. Wang, X. Sun, *Energy Environ. Sci.*, 8 (2015) 1110-1138.
35. B. Wang, W. Al Abdulla, D. Wang, X. S. Zhao, *Energy Environ. Sci.*, 8 (2015) 869-875.
36. Y. Wang, Z. Feng, J. Chen, C. Zhang, *Mater. Lett.*, 71 (2012) 54-56.
37. K. Zhang, J. T. Lee, P. Li, B. Kang, J. H. Kim, G. R. Yi, J. H. Park, *Nano Letters*, 15 (2015) 6756-6763.
38. Y. Zhang, H. J. Zhang, Y. Y. Feng, L. Fang, Y. Wang, *Small*, 12 (2016) 516-523.